Thermometry of Silicon Nanoparticles

Matthew Mecklenburg, Brian Zutter, and B. C. Regan

Thermometry of Silicon Nanoparticles

Matthew Mecklenburg*
Center for Electron Microscopy and Microanalysis,
University of Southern California, Los Angeles, California 90089, USA

Brian Zutter and B. C. Regan†
Department of Physics & Astronomy and California NanoSystems Institute,
University of California, Los Angeles, California 90095 USA
(Dated: December 11, 2017)

Current thermometry techniques lack the spatial resolution required to see the temperature gradients in typical, highly-scaled modern transistors. As a step toward addressing this problem, we have measured the temperature dependence of the volume plasmon energy in silicon nanoparticles from room temperature to 1250°C, using a chip-style heating sample holder in a scanning transmission electron microscope (STEM) equipped with electron energy loss spectroscopy (EELS). The plasmon energy changes as expected for an electron gas subject to the thermal expansion of silicon. Reversing this reasoning, we find that measurements of the plasmon energy provide an independent measure of the nanoparticle temperature consistent with that of the heater chip's macroscopic heater/thermometer to within the 5% accuracy of the chip thermometer's calibration. Thus silicon has the potential to provide its own, high-spatial-resolution thermometric readout signal via measurements of its volume plasmon energy. Furthermore, nanoparticles in general can serve as convenient nanothermometers for *in situ* electron microscopy experiments.

I. INTRODUCTION

Silicon, as the primary constituent of most semiconductor devices, is perhaps the most important and most studied material in modern technology. Silicon's thermal properties are particularly relevant to the design of devices such as microprocessors, since heat transport is frequently a performance-limiting factor in highly-scaled and high-power density electronics [1, 2]. The current semiconductor processing node, designated with the scale label '10-nm', produces devices with features that are even smaller (in the vertical direction) and multiple, nontrivial interfaces.

As such devices approach the atomic limit, classical, continuum thermal transport theory breaks down [1, 3]. Improved designs for next-generation microprocessors, memory, and opto-electronics will come with a better understanding of thermal transport at these small length scales. To gain this understanding, thermometry techniques with $\lesssim 1\,\mu$m spatial resolution are required. However, no currently available technique can resolve the thermal gradients within the smallest modern transistors.

The temperature mapping techniques of most relevance to microelectronics are generally either optical or scanning-probe [1, 4]. Optical examples include micro-Raman and thermoreflectance [5–7], both of which are diffraction-limited to 500–1000 nm spatial resolution. Mechanical scanning thermal microscopy (SThM) techniques do better by rastering a sharp tip across a sample [8, 9]. They extract a thermometric signal by analyzing a tip-embedded thermometer [10–12], the heat transfer

between the tip and sample [10, 13], or the thermal expansion of the sample [14].

We are developing a temperature mapping technique, plasmon energy expansion thermometry (PEET) [15], with the capability for $\lesssim 10$ nm spatial resolution inside a thermometric material. The technique is scanning, but, unlike most scanning techniques, it is non-contact in the sense that the heat transfer between the probe and the sample is negligible. PEET infers a material's temperature from measurements of its volume plasmon energy. The plasmon energy, $E_p = \hbar\sqrt{e^2 n/\epsilon_0 m}$ in the electron gas model (where e and m are the electronic charge and mass respectively), gives the valence electron density n. The electron density in turn indicates the temperature via the material's coefficient of thermal expansion (CTE), which is determined separately. In a scanning transmission electron microscope (STEM) equipped with electron energy loss spectroscopy (EELS), E_p can be mapped with sufficiently high spatial resolution to observe the density changes at grain boundaries [15]. Thus temperature mapping with resolution approaching the atomic limit can be achieved.

In this communication we share two main results. First, we have measured the temperature dependence of silicon's bulk plasmon energy, which has not been reported previously. This measurement is a necessary step toward the goal of applying PEET to determine the temperature gradients within an operating transistor, using the transistor's own silicon as the thermometric read-out material.

Second, we show how nanoparticles can serve as fiducial thermometers for *in situ* TEM experiments. A compact PEET thermometer in or near the TEM field of view (FOV) can provide an improved temperature determination without the complications of external wiring or addi-

* matthew.mecklenburg@usc.edu
† regan@physics.ucla.edu

tional thermal loading. Nanoparticles are small and can be easily dispersed. With a variety of nanoparticles commercially available (*e.g.* silicon, aluminum, indium, and tungsten), the specific type can be chosen to best meet the experiment's requirements (*e.g.* operating temperature range and chemical compatibility). Similar ideas for fiducial thermometers have been implemented previously in an optical context, for instance with nitrogen-vacancy centers in diamond [16] or lanthanide ion-doped nanocrystals [17]. The PEET approach allows implementation in a TEM, and without requiring any additional hardware more exotic than a standard EELS spectrometer. In a sense each nanoparticle serves as an expansion thermometer in the style of Fahrenheit's mercury-in-glass design, but with a construction that is much simpler, cheaper, and smaller (vs., for example, the approach of Ref. 18).

II. EXPERIMENT

To accomplish these two goals we measured the plasmon energy in silicon nanoparticles as a function of temperature using a chip-style TEM-sample heating holder (DENS Solutions Wildfire S3, Fig. 1 *top*). Relative to furnace-type heating holders, this type of holder equilibrates faster, drifts less, consumes less power, and provides more accurate temperature read-out [19]. As shown in Fig. 1 (*top*), each chip had a $300\,\mu$m$\times300\,\mu$m, SiN$_x$-encapsulated, spiral Joule heater/thermometer atop a silicon nitride membrane with nearby < 20 nm-thick, $100\,\mu$m^2 electron-transparent windows [19, 20]. The specifications for these chips list a guaranteed temperature range of room temperature to $1{,}300°$C, a maximum temperature of $1{,}500°$C, achievable temperature change rates of $200°$C/ms, and settling times of < 2 s. At $1250°$C (1523 K) the heater drew 6.5 mA at 2.7 V, dissipating 18 mW.

The window temperature was determined via a four-wire measurement of the heater resistance, which had been calibrated vs. temperature by the manufacturer to an accuracy of 5%. By design the chip featured a temperature gradient, with the temperatures of different windows varying by more than 15% relative to the difference from ambient at a given heater power. The temperature calibration was only accurate for the windows nearest the center of the heater.

Samples were prepared by dropcasting silicon nanoparticles from $1\mu l$ of an ethanol solution onto a chip (Figure 1). According to the vendor (SkySpring Nanomaterials), the nanoparticles were manufactured by chemical vapor deposition (CVD), had 99% purity, and a 100 nm average particle size.

Generally speaking, 100 nm is roughly one mean-free path for plasmon production, so nanoparticles of this thickness are preferred for PEET. Particle size-dependent effects are a potential source of systematic errors, but these only appear in much smaller particles. For in-
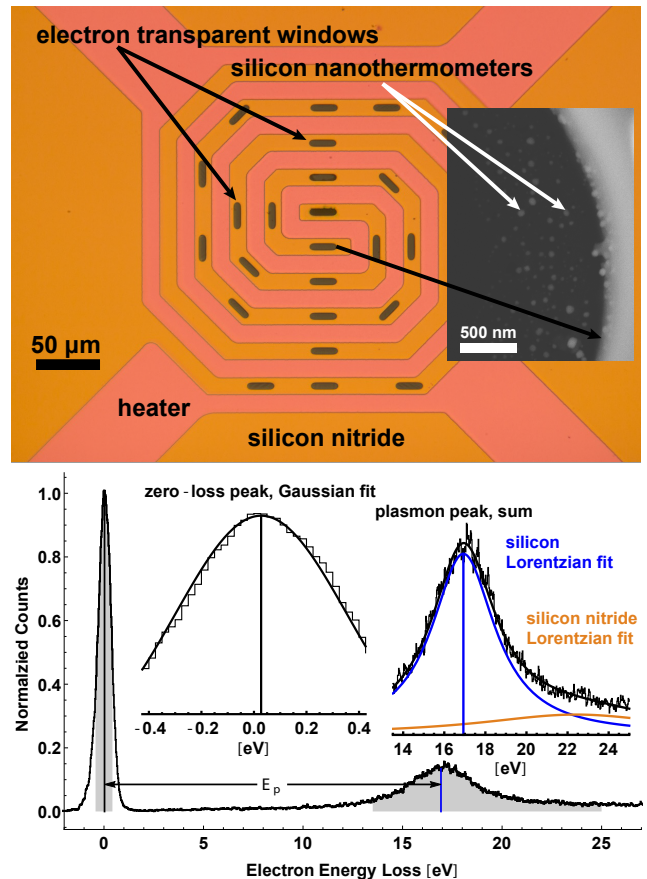

FIG. 1. (*top*) Chip-style TEM-sample heater. This optical micrograph shows the spiral heater and its four leads, which are used to make the resistance measurement that forms the basis of the chip's temperature determination. At temperature the windows nearer the center of the spiral are hotter than those towards the edge, which emphasizes the desirability of having a small, local thermometer in the FOV. A scanning electron micrograph (inset) shows a typical dispersion of nanoparticles near the edge of one of the oblong, electron-transparent windows, and highlights the enormous size difference between these nanothermometers and the chip's dual-function heater/thermometer. (*bottom*) Low-loss EELS from a silicon nanoparticle. The ZLP, silicon, and the silicon nitride plasmon peaks are fit to Gaussian, Lorentzian, and Lorentzian functions respectively (insets) using data from the energy windows indicated by the grey vertical bands.

stance, the bulk plasmon resonance has been observed to change in silicon nanoparticles with diameters $\lesssim 10$ nm [21]. Similarly, size-dependent melting effects, which likely would have concomitant effects on the CTE, are only seen in particles with diameters $\lesssim 15$ nm [22].

EELS spectrum images of silicon nanoparticles at different temperatures were acquired in a JEOL JEM-2100F TEM equipped with a Gatan Quantum SE GIF. The microscope was operated at 80 kV with a beam current of 100 pA, a 0.5 nm probe, and a convergence semi-angle of 12 mrads. (The 80 kV accelerating voltage enhances
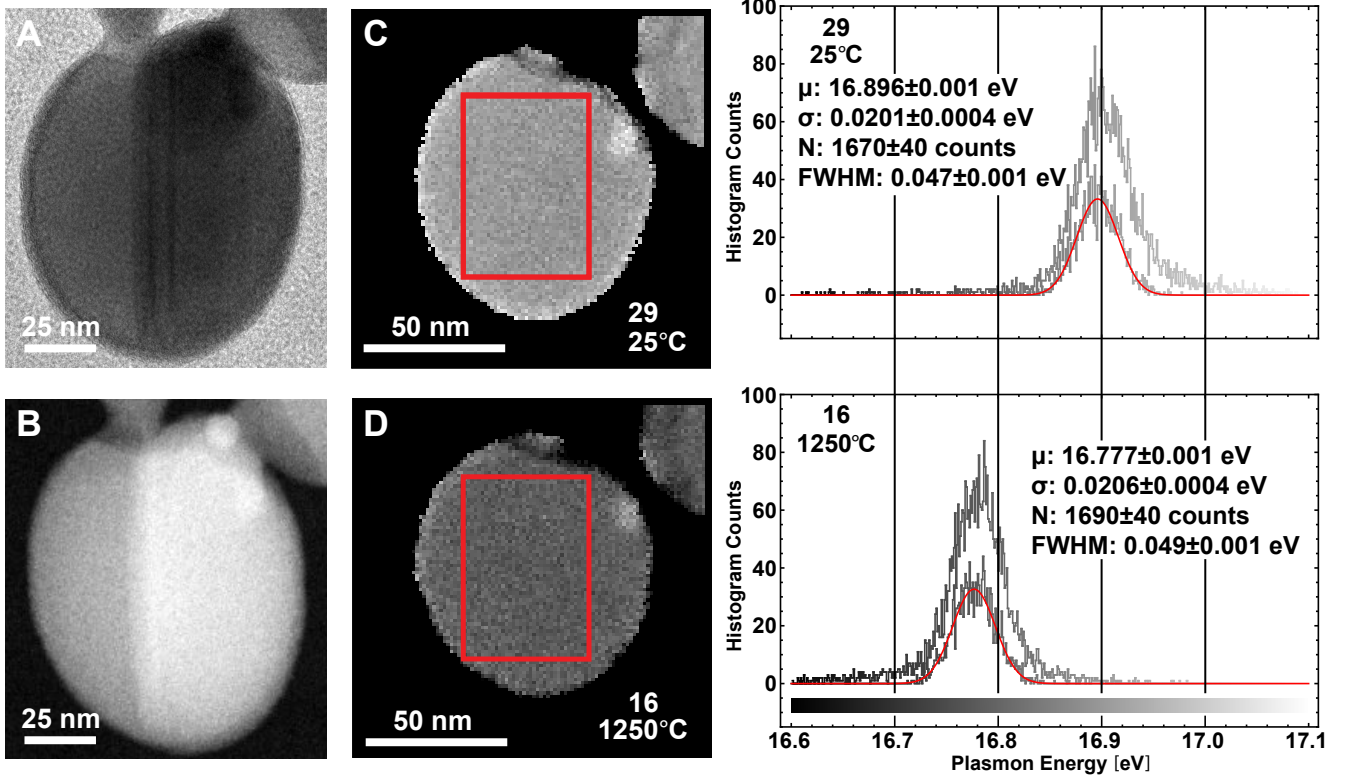
FIG. 2. (A) TEM image of a silicon nanoparticle with at least two grains and an oxide coating. (B) Dark-field STEM image of the same nanoparticle. (C) and (D) Plasmon energy maps of the nanoparticle at 25°C and 1250°C respectively (the point number is listed above the temperature — see Fig. 3). The combined scale bar/histograms to the right show the distributions for the entire FOV, and the indicated red ROI. The latter is fit to a Gaussian function.

the plasmon production rate by roughly a factor of two relative to the rate at 200 kV.) The spectrometer collected 64 spectra per second with a semi-collection angle of 20 mrad, a 2.5 mm entrance aperture, a dispersion of 25 meV/channel, and 26× vertical binning.

In each spectrum the silicon plasmon energy was determined by fitting the zero loss peak (ZLP), the silicon nitride plasmon peak, and the silicon plasmon peak, as shown in Fig. 1. Fitting the ZLP with a Gaussian function in a fit window of full-width 0.85 eV centered around the spectrum maximum returned a full-width at half-maximum (FWHM) of 0.76 ± 0.01 eV. In a region of interest (ROI) bare of any material but the electron-transparent membrane, the silicon nitride plasmon peak was fit with a Lorentzian function in a fit window extending from 19.5 to 26.5 eV relative to the ZLP center. The peak center and width from this fit were then fixed, and a two-Lorentzian fit in the window 13.5–25.0 eV was performed over the entire FOV. This fit had four free parameters: the amplitude of the silicon nitride peak, and the amplitude, center, and width of the silicon peak. The difference between the silicon peak center and the ZLP center is taken to be the silicon plasmon energy [15].

III. RESULTS

Typical data extracted from a 90 nm-diameter silicon nanoparticle are shown in Figure 2. The TEM image with its diffraction contrast reveals the most detailed structural information, showing the nanoparticle's 3–5 nm-thick oxide coating and two distinct crystal grains. The high-angle annular dark field STEM image shows the grains only, while the plasmon energy maps show none of these features and are basically uniform. Including the fit of the silicon nitride peak in the data analysis is necessary to achieve this uniformity; without it, the plasmon energies within 10 nm of the nanoparticle edge appear to be systematically higher than those in the interior (the low-amplitude silicon plasmon gets pulled higher by the slope in the silicon nitride background). Histograms of the silicon plasmon energies are well-fit by Gaussian distributions.

Converting these plasmon energy differences into temperature differences requires integrating silicon's linear CTE $\alpha(T) \equiv (1/l)(dl/dT)$, where l is a length in the material [23]. The plasmon energies E_p at an unknown temperature T and the known reference temperature T_0 are related to the CTE by the ratio $R \equiv$

$[E_p(T) - E_p(T_0)]/E_p(T_0)$, where

$$R \simeq -\frac{3}{2}\left(\frac{l - l_0}{l_0}\right) \simeq -\frac{3}{2}\int_{T_0}^{T}\alpha(T')dT'. \qquad (1)$$

Okada and Tokumaru [24] provide an empirical formula for the CTE, valid between 120 and 1500 K, which integrated gives (for T' in kelvin)

$$\int \alpha(T')dT' = (1313.41e^{-0.00588T'}$$
$$+ 3.725T' + 0.0002774T'^2) \times 10^{-6}. \quad (2)$$

At $T = 300, 600, 900, 1200,$ and 1500 K, this expression gives the CTE $\alpha = 2.57, 3.83, 4.19, 4.38,$ and 4.56 (all $\times 10^{-6}$) respectively, which is to say that silicon's CTE is consistently increasing with temperature, though more slowly after a shoulder in the neighborhood of 700 K. (Regarding PEET's sensitivity in silicon, it is unfortunate that, compared to that of other materials, silicon's high-temperature CTE is small, smaller even than that of diamond [23].) In the range 298 to 1500 K the integrated CTE $f(T) \equiv \int_{T_0}^{T}\alpha(T')dT' \simeq \alpha_1\Delta T + \alpha_2\Delta T^2$ ranges from 0 to 4.85×10^{-3} and is approximated with the coefficients $\alpha_1 = 3.25 \times 10^{-6}$ K^{-1} and $\alpha_2 = 6.84 \times 10^{-10}$ K^{-2}, where $\Delta T \equiv T - T_0$ and $T_0 = 298$ K. (For comparison, in aluminum the corresponding numbers [15] are $\alpha_1 = 23.5 \times 10^{-6}$ K^{-1} and $\alpha_2 = 89 \times 10^{-10}$ K^{-2} in the range 25 to 650°C.) However, while the quadratic approximation to Eq. 2 is good to better than 5×10^{-5} through the whole range, the relative errors are as large as 27% near room temperature where $f(T)$ is small. Since for many applications the lower end of the range will be the most interesting region, we invert $f(T)$ numerically to find temperatures.

Roughly speaking, silicon's plasmon shifts -0.1 meV/K. Even a 1200 K temperature change produces a peak shift that is barely discernible by eye [25]. For the data in Fig. 2 the measured standard deviation of the single-pixel plasmon energies is 20 meV, which corresponds to a 200 K shift. With such uncertainties, meaningful temperatures cannot be calculated at the single-pixel level; the integrated CTE $f(T)$ is valid over only a limited temperature range. Furthermore, $f(T)$ is non-linear. Thus the operations of computing the temperature from the plasmon energies and averaging over some ROI do not commute — the averaging must be done first. To suppress systematic errors arising from a weak silicon plasmon signal, we compute the mean plasmon energy $\overline{E_p}(T)$ for an ROI in the interior of the nanoparticle at the unknown temperature T. Finding the corresponding mean energy $\overline{E_p}(T_0)$ in a similar ROI in a map acquired at the reference temperature T_0, we calculate $-2\overline{R}/3 = f(T)$ and then invert to find the temperature.

The nanoparticle plasmon energy maps shown in Fig. 2 represent two data points in a temperature scan designed to demonstrate the utility of such nanoparticles as nanothermometers. (For a more comprehensive view of the
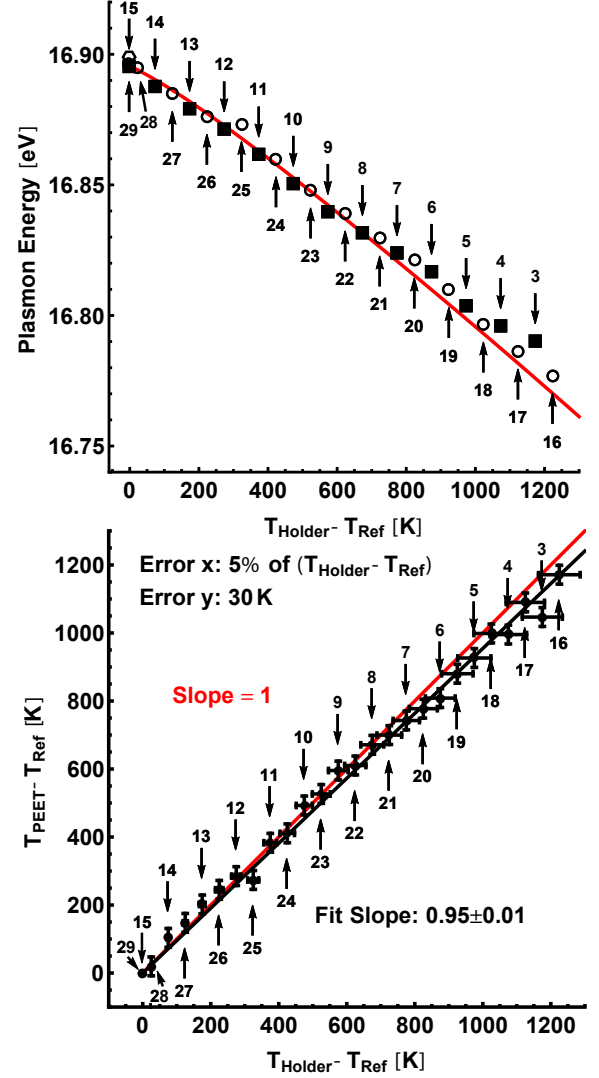

FIG. 3. *(top)* The plasmon energy averaged over the ROI indicated in Fig. 2 is plotted as a function of the holder temperature. Four ambient temperature measurements are shown (points labeled 1, 2, 15, and 29), along with two separate, high-to-low temperature ramps (black squares, 3–14, and open circles, 16–28, respectively). The measured plasmon energy changes follow the curve calculated using silicon's CTE. *(bottom)* The corresponding PEET temperatures agree with the holder's temperature determination to within its stated 5% accuracy.

entire dataset see [25].) This particular scan consisted of two room temperature data points, followed by two ramps down from high temperature to room temperature in 100°C steps (according to temperature as determined by the holder), with the first ramp beginning at 1200°C and the second at 1250°C. Interleaving two ramps with 100°C steps, as opposed performing a single ramp with 50°C steps, gives an important indication of the stability of the nanoparticles with respect to thermal cycling and repeated STEM imaging. For maximum utility as

nanothermometers, the nanoparticles should be robust to both perturbations.

The results of this scan are shown in Fig. 3. The plasmon energy versus temperature plot shows a total shift in the plasmon energy of 120 meV — a mere 3% of the peak's 3.7 eV FWHM — across the entire measured range between room temperature and 1523 K, highlighting the necessity of using curve-fitting to extract the thermometric signal. The plasmon energies determined in the two interleaved temperature ramps are themselves gratifyingly interleaved, showing no significant systematic shift between the first and second ramps. To estimate the error in the PEET determination, we require that the χ^2 per degree of freedom in the linear fit of Fig. 3 be unity, which gives a PEET error of 30 K. (Standard error propagation applied to the invertible, quadratic approximation to $f(T)$ gives errors that are too small by a factor of 8 for reasons that are not presently understood.) The four separate room-temperature plasmon energy measurements have a standard deviation of 2 meV, an energy shift which is equivalent to 20 K. This value gives an additional measure of the error in PEET's temperature determination that is of the same order as the first. Comparing the temperatures derived from resistance measurements of the chip's 300 μm heater/thermometer to those derived from PEET applied to the 90 nm silicon nanoparticle, we find that they agree at the 5% level, the stated accuracy of the chip's temperature calibration.

IV. DISCUSSION

While applying PEET to nanoparticles we encountered various pitfalls, but the problems were usually easily recognized and even quantifiable. A change in the experimental parameters between the first and the last ambient-temperature measurements warns of a possible systematic error. (Of course taking both measurements, and more within an experiment if possible, is a necessary part of a sound experimental protocol.) In cases with independent thermometers, like the one described here, this warning might be unrelated to PEET and concern the other thermometer instead. For instance, a change in the zero-power resistance of a heater/thermometer indicates that it has been damaged, either through use or through processing (*e.g.* plasma cleaning), and that its temperature calibration can no longer be considered reliable. In other cases the problem concerns PEET: the nanoparticle might change, either in its morphology, its plasmon energy, or both. We have seen evidence of alloying or doping within a heating experiment, and also signs of beam-induced damage. Aberration-corrected microscopes are particularly hazardous in the latter regard, for a total beam current that is harmless in an uncorrected probe can, concentrated, radically transform a nanoparticle, making it useless for thermometry. Whatever the source of the change, the shift in a nanoparticle's plasmon energy under nominally identical conditions gives

a quantitative measure of the magnitude of a potential systematic error.

In addition to the systematic errors already mentioned, we have also considered the effects of beam heating, departure from thermal equilibrium, and non-thermal strain. Beam heating occurs because the electron beam carries a power of 80 kV×100 pA = 8μW, and about half of the electrons lose energy to the sample. However, most of this loss is via plasmon production, which deposits only 17 eV per electron. Thus the deposited power is only $\sim$ 1 nW. Unless the object being probed has exceptional thermal isolation, such a tiny power input produces a negligible temperature change. For instance, depositing 1 nW into a nanoparticle with a 1 W/m · K thermal barrier that is 5 nm thick (*e.g.* a silicon dioxide shell) and contacted through a (conservative) area of 5 nm^2 gives an unresolvable 1 K temperature shift. In the rare case of a poorer thermal connection, the problem is evident, for the beam depresses the reference temperature plasmon energy from the expected value, or, in extreme instances, melts the particle.

It is worth considering whether beam heating could compromise the PEET determination of the local equilibrium temperature by driving the plasmons to a temperature different from that of the lattice. According to our understanding, a brief departure from thermal equilibrium does occur, but it does not compromise the temperature measurement. PEET measures the plasmon energy, which depends on the equilibrium lattice temperature via thermal expansion. PEET does not measure the plasmon temperature. This point is crucial, for a plasmon is not in thermal equilibrium with the lattice. Viewing the plasmons as a collection of quantum harmonic oscillators with energy $E_p = 17$ eV and employing the Einstein model, we see that the plasmons have essentially zero heat capacity, since $e^{-E_p/kT}$ is a very small number at the temperatures studied. The oscillators are all frozen out, and no plasmons are present without excitation by the beam. Creating even one 17 eV quantum drives the plasmon gas far from thermal equilibrium. This departure from equilibrium is short-lived, however. The FWHM of the plasmon peak $\sim$ 4 eV implies a plasmon lifetime of $\sim$ 0.1 fs via the uncertainty relation. With a 100 pA beam current, the time between beam electrons passing through the sample is 1.6 ns. So the departure from thermal equilibrium occurs during a period of time that represents about one part in 10^7 of the total.

Non-thermal strain will present a challenge for this thermometry technique, especially in the active transistor application envisioned, which may require modeling to account for the geometric constraints on free thermal expansion. Even in the simple nanoparticle case presented here, strain effects may be comparable to our sensitivity. Modeling the nanoparticle as a spherical silicon core surrounded by a continuous, silicon dioxide shell [26], one can estimate the deviation in the silicon's strain

$\Delta\epsilon$ from the free thermal expansion case as

$$\Delta\epsilon \simeq \frac{(\alpha_{\text{ox}} - \alpha_{\text{Si}})\Delta T}{1 + \frac{E_{\text{Si}}}{(1-2\nu_{\text{Si}})E_{\text{ox}}}\frac{a^3(1-2\nu_{\text{ox}})+b^3(1+\nu_{\text{ox}})/2}{b^3-a^3}} \quad (3)$$

where the α's, ν's, and E's refer to the respective CTE's, Poisson's ratios, and Young's moduli, ΔT is the temperature change, and a and b are the inner and outer radii of the oxide shell that would obtain under free thermal expansion. Since $\alpha_{\text{ox}} < \alpha_{\text{Si}}$, we expect the oxide shell to exert a compressive force on the core as the nanoparticle warms, leading to denser silicon and a systematic underestimate of the temperature. Using standard values for the materials properties ($\alpha_{\text{ox}} = 5.6\times10^{-7}$, $\alpha_{\text{Si}} = 2.6 \times 10^{-6}$, $E_{\text{ox}} = 70$ GPa, $E_{\text{Si}} = 160$ GPa, $\nu_{\text{ox}} = \nu_{\text{Si}} = 0.17$), and the dimensions $a = 42$ nm and $b = 46$ nm for the particle shown in Fig. 2, we find an expected strain error $\Delta\epsilon/\alpha_{\text{Si}}\Delta T \simeq -5\%$, comparable to our uncertainty.

While for the data shown in Fig. 3 a correction would improve the agreement between the PEET value and the holder temperature, we do not feel that such a correction is warranted. As a function of the radial coordinate r, the membrane stress generated in the shell is

$$\sigma_{\theta\theta} = \sigma_{\phi\phi} = \frac{P_a a^3}{b^3 - a^3}(1 + b^3/2r^3), \quad (4)$$

where the pressure P_a exerted on the oxide shell from the inside is $E_{\text{Si}}\Delta\epsilon/(1 - 2\nu_{\text{Si}})$. Thus for a $\Delta T = 1000$ K we expect, in the constant CTE approximation, a membrane tensile stress in the oxide of 160 MPa, and a strain of 0.2%. (The radial stress is compressive and five times smaller.) Silica has a tensile strength that can vary over orders of magnitude [27, 28], depending on the purity, growth method, and subsequent handling. Unless the native oxide shell is high quality silica, it will fracture during heating, allowing for free expansion. Furthermore, Eq. 3 predicts even larger effects in aluminum, where the CTE difference and oxide Young's modulus are bigger. We have seen no sign of this strain effect in aluminum nanoparticles. Presently we believe that the oxide shells lack structural integrity, and thus this strain effect is negligible. However, for precision PEET this topic warrants further study.

ACKNOWLEDGMENTS

[1] Ralf Heiderhoff, Andreas Makris, and Thomas Riedl, "Thermal microscopy of electronic materials," Materials Science in Semiconductor Processing **43**, 163–176 (2016).

[2] David G. Cahill, Paul V. Braun, Gang Chen, David R. Clarke, Shanhui Fan, Kenneth E. Goodson, Pawel Keblinski, William P. King, Gerald D. Mahan, Arun Majumdar, Humphrey J. Maris, Simon R. Phillpot, Eric Pop, and Li Shi, "Nanoscale thermal transport. II. 2003–2012," Applied Physics Reviews **1**, 011305 (2014).

[3] H. B. G. Casimir, "Note on the conduction of heat in crystals," Physica **5**, 495–500 (1938).

[4] Myeongsub Mike Kim, Alexandre Giry, Mohammad Mastiani, Gustavo O. Rodrigues, Alessandro Reis, and Philippe Mandin, "Microscale thermometry: A review," Microelectronic Engineering Micro/Nano Emerging Technologies 2015, **148**, 129–142 (2015).

[5] K. Maize, G. Pavlidis, E. Heller, L. Yates, D. Kendig, S. Graham, and A. Shakouri, "High Resolution Thermal Characterization and Simulation of Power AlGaN/GaN HEMTs Using Micro-Raman Thermography and 800 Picosecond Transient Thermoreflectance Imaging," in *2014 IEEE Compound Semiconductor Integrated Circuit Symposium (CSICs)* (2014) pp. 1–8.

[6] T. Beechem, A. Christensen, S. Graham, and D. Green, "Micro-Raman thermometry in the presence of complex stresses in GaN devices," Journal of Applied Physics **103**, 124501 (2008).

[7] Peter-Wolfgang Epperlein, "Micro-Temperature Measurements on Semiconductor Laser Mirrors by Reflectance Modulation: A Newly Developed Technique for Laser Characterization," Japanese Journal of Applied Physics **32**, 5514–5522 (1993).

[8] A. Majumdar, "Scanning Thermal Microscopy," Annual Review of Materials Science **29**, 505–585 (1999).

[9] Séverine Gomès, Ali Assy, and Pierre-Olivier Chapuis, "Scanning thermal microscopy: A review," physica status solidi (a) **212**, 477–494 (2015).

[10] C. C. Williams and H. K. Wickramasinghe, "Scanning thermal profiler," Applied Physics Letters **49**, 1587–1589 (1986).

[11] G. Mills, H. Zhou, A. Midha, L. Donaldson, and J. M. R. Weaver, "Scanning thermal microscopy using batch fabricated thermocouple probes," Applied Physics Letters **72**, 2900–2902 (1998).

[12] Kyeongtae Kim, Wonho Jeong, Woochul Lee, and Pramod Reddy, "Ultra-High Vacuum Scanning Thermal Microscopy for Nanometer Resolution Quantitative Thermometry," ACS Nano **6**, 4248–4257 (2012).

[13] Fabian Menges, Philipp Mensch, Heinz Schmid, Heike Riel, Andreas Stemmer, and Bernd Gotsmann, "Temperature mapping of operating nanoscale devices by scanning probe thermometry," Nature Communications **7**, 10874 (2016).

[14] A. Majumdar and J. Varesi, "Nanoscale Temperature Distributions Measured by Scanning Joule Expansion Microscopy," Journal of Heat Transfer **120**, 297–305 (1998).

[15] Matthew Mecklenburg, William A. Hubbard, E. R.

White, Rohan Dhall, Stephen B. Cronin, Shaul Aloni, and B. C. Regan, "Nanoscale temperature mapping in operating microelectronic devices," Science **347**, 629–632 (2015).

[16] G. Kucsko, P. C. Maurer, N. Y. Yao, M. Kubo, H. J. Noh, P. K. Lo, H. Park, and M. D. Lukin, "Nanometre-scale thermometry in a living cell," Nature **500**, 54–58 (2013).

[17] Fiorenzo Vetrone, Rafik Naccache, Alicia Zamarrón, Angeles Juarranz de la Fuente, Francisco Sanz-Rodríguez, Laura Martinez Maestro, Emma Martín Rodriguez, Daniel Jaque, José García Solé, and John A. Capobianco, "Temperature Sensing Using Fluorescent Nanothermometers," ACS Nano **4**, 3254–3258 (2010).

[18] Yihua Gao and Yoshio Bando, "Nanotechnology: Carbon nanothermometer containing gallium," Nature **415**, 599–599 (2002).

[19] Luigi Mele, Stan Konings, Pleun Dona, Francis Evertz, Christoph Mitterbauer, Pybe Faber, Ruud Schampers, and Joerg R. Jinschek, "A MEMS-based heating holder for the direct imaging of simultaneous in-situ heating and biasing experiments in scanning/transmission electron microscopes," Microscopy Research and Technique **79**, 239–250 (2016).

[20] L. Mele, F. Santagata, E. Iervolino, M. Mihailovic, T. Rossi, A. T. Tran, H. Schellevis, J. F. Creemer, and P. M. Sarro, "A molybdenum MEMS microhotplate for high-temperature operation," Sensors and Actuators A: Physical Selected papers from The 16th International Conference on Solid-State Sensors, Actuators and Microsystems, **188**, 173–180 (2012).

[21] M. Mitome, Y. Yamazaki, H. Takagi, and T. Nakagiri, "Size dependence of plasmon energy in Si clusters," Journal of Applied Physics **72**, 812–814 (1992).

[22] Makoto Hirasawa, Takaaki Orii, and Takafumi Seto, "Size-dependent crystallization of Si nanoparticles," Applied Physics Letters **88**, 093119 (2006).

[23] Glen A. Slack and S. F. Bartram, "Thermal expansion of some diamondlike crystals," Journal of Applied Physics **46**, 89–98 (1975).

[24] Yasumasa Okada and Yozo Tokumaru, "Precise determination of lattice parameter and thermal expansion coefficient of silicon between 300 and 1500 K," Journal of Applied Physics **56**, 314–320 (1984).

[25] See Supplemental Material at [URL will be inserted by publisher] for additional figures (Part 1) and maps of the fit parameters (Part 2).

[26] Allan Bower, *Applied Mechanics of Solids* (CRC Press, Boca Raton, 2009).

[27] Andri M. Gretarsson, "References for tensile strength of vitreous silica fibers at room temperature," arXiv:cond-mat/0205448 (2002).

[28] Sanjib C. Chowdhury, Robert M. Elder, Timothy W. Sirk, Bazle Z. Haque, Jan W. Andzelm, and John W. Gillespie, "Molecular dynamics study of the mechanical properties of silica glass using ReaxFF," Proceedings of the American Society for Composites: Thirty-First Technical Conference (2016).